

*Supporting Information for*

**Hierarchical layered nickel-iron double hydroxide/ carbon nanotube  
fiber electrode for constructing asymmetric fiber supercapacitor**

Hao Geng<sup>1\*</sup>, Yuanqiang Song<sup>2\*</sup>, Wei Luo<sup>3</sup>, Yan Zhou<sup>4</sup>, Yali Li<sup>1</sup>

<sup>1</sup> Advanced Carbon Materials Research Center, School of Materials Science and Engineering,  
Changzhou University, Changzhou 213164, P.R. China

<sup>2</sup> Institute of Flexible Electronics Technology of Tsinghua, 314001, Jiaxing, P.R. China

<sup>3</sup> School of Material Science and Technology, Luoyang Institute of Science and Technology,  
Luoyang 471023, P.R. China

<sup>4</sup> Key Laboratory for Soft Chemistry and Functional Materials of Ministry of Education, Nanjing  
University of Science and Technology, Nanjing 210094, P.R. China

\*Corresponding author, [E-mail: ghaosiccas@cczu.edu.cn](mailto:ghaosiccas@cczu.edu.cn)

[E-mail: songyuanqiang@ifet-tsinghua.org](mailto:songyuanqiang@ifet-tsinghua.org)

## Clarification of equations used for evaluating the energy storage ability of battery-like electrode materials

Usually, the equation (1) provided in the manuscript is suitable for calculating the capacity of the EDLC material which stores energy by accumulation of charges through electrostatic interactions at the electrode–electrolyte interface and the pseudocapacitive material (such as MnO<sub>2</sub>) which display an electrochemical behavior typical of that observed for a capacitive carbon electrode in mild aqueous electrolyte [1,2].

Correspondingly, the charge/discharge curves of EDLC and pseudocapacitive material always present (quasi)triangular shape. While in this work, the electrochemical characteristics (obvious redox peak and discharge plateau) of Ni-Fe LDH@CNTF present distinct behaviors from the EDLC material or pseudocapacitive material. According to definition and concept of pseudocapacitance proposed by Conway, it can be inferred that Ni-Fe LDH@CNTF is actually belong to battery-like material which exhibit typical faradaic behavior. Based on this, the equation of batteries to calculate the capacity should be adopted in current situation to avoid the deviation from the real values. Therefore, the specific capacity ( $C_c$ , mAh/g) of battery-type Ni-Fe LDH@CNTF was calculated from the GCD curves by the following Equation S1 [3]:

$$C_c = \frac{I \times \Delta t}{m} \quad (\text{S1})$$

Before evaluating the electrochemical performance of ASC device, the charge balance between two electrode was processed based on the following equation [4,5]:

$$C_{c+} \times m_+ = C_{s-} \times m_- \times \Delta V_- / 3.6 \quad (\text{S2})$$

where  $C_{c+}$  (mAh/g) and  $m_+$  (g) are the mass and specific capacity of the positive electrode, while  $C_{s-}$  (F/g),  $m_-(g)$ ,  $\Delta V_-(V)$  are the mass, specific capacitance and operating potential window of the negative electrode, respectively.

### **Charge transfer mechanisms simulation**

The charge transfer mechanisms and electrode kinetics were investigated by Dunn's method. [6–9] To quantify the ratio of capacitive contribution of present AFSC from the total capacity, the formula can be divided into two parts quantitatively as follows:

$$i(\nu) = k_1\nu + k_2\nu^{1/2} \quad (S3)$$

where  $k_1$  and  $k_2$  represent the scan rate independent constants;  $\nu$  is the scan rates,  $k_1\nu$  represents capacitance contribution and  $k_2\nu^{1/2}$  represents contribution coming from diffusion-controlled Faradaic processes.

## Results

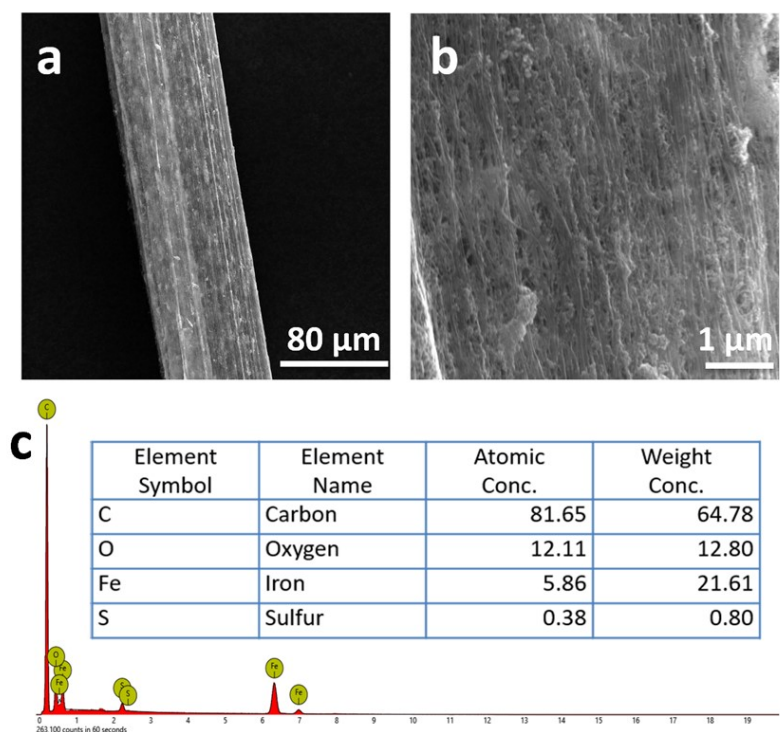


Figure S1. SEM images of original CNTF observed at low magnification (a) and high magnification(b); (c) Corresponding EDX of CNTF.

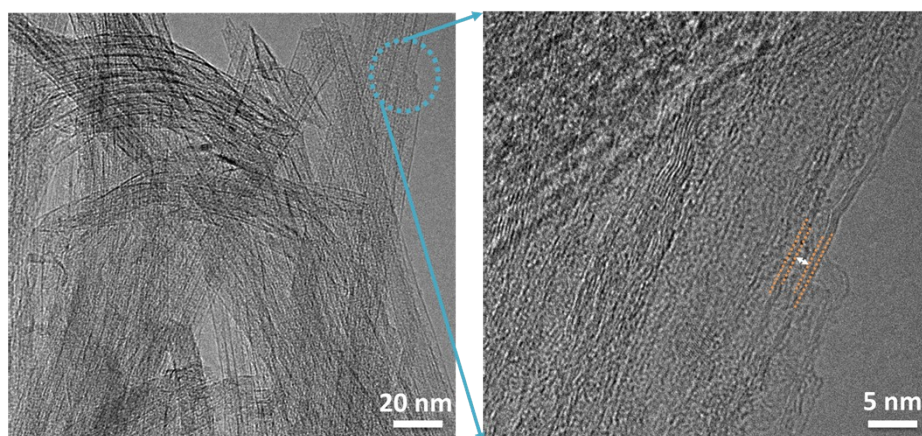


Figure S2. TEM morphologies of original CNTF indicating the major component of CNT bundles.

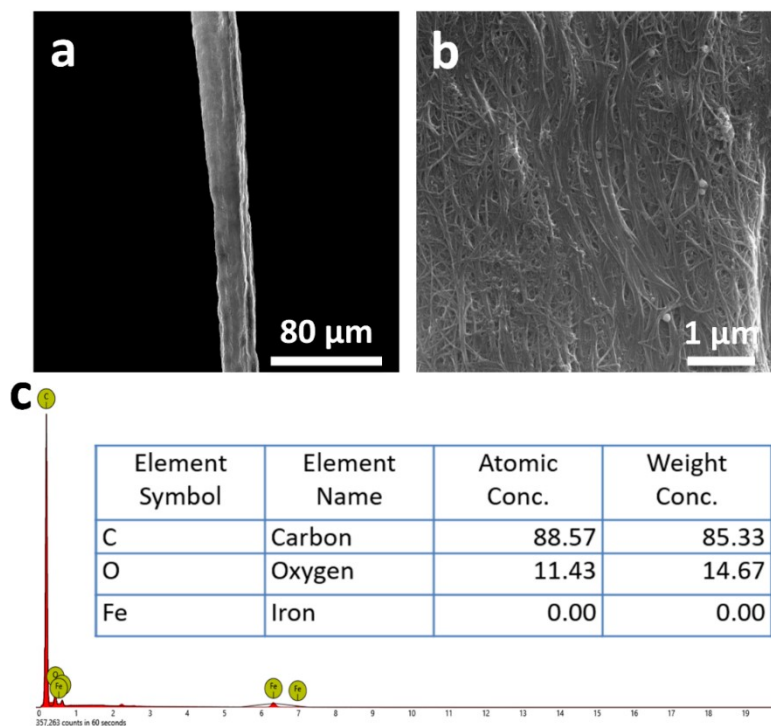


Figure S3. SEM images of acid treated CNTF observed at low magnification (a) and high magnification(b); (c) Corresponding EDX of acid treated CNTF.

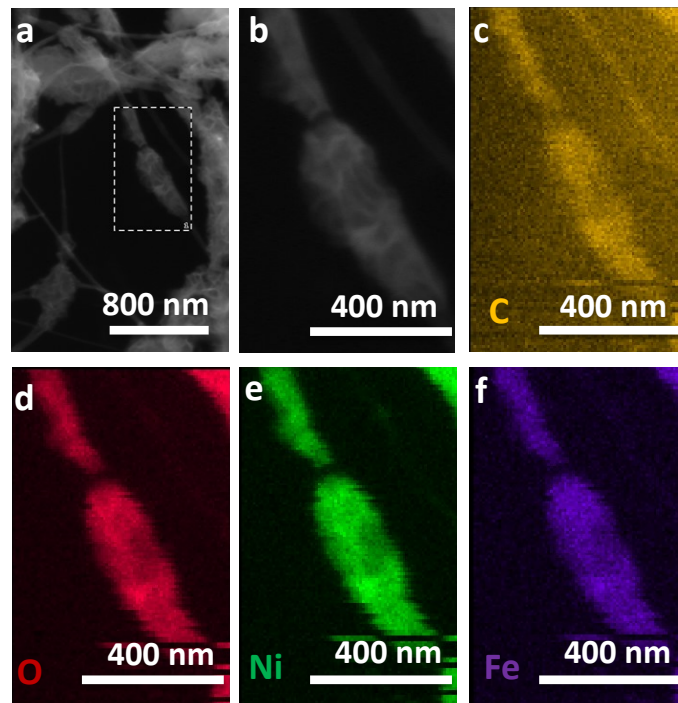


Figure S4. (a) Low magnification and (b) high magnification SEM images of Ni-Fe LDH grown on single CNT; (c-f) Corresponding C, O, Ni and Fe elements mapping.

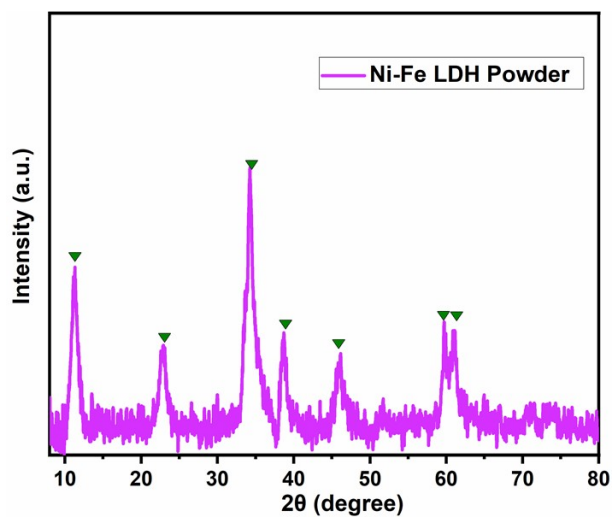


Figure S5. XRD pattern of Ni-Fe LDH powder (hydrothermal reaction time: 24h).

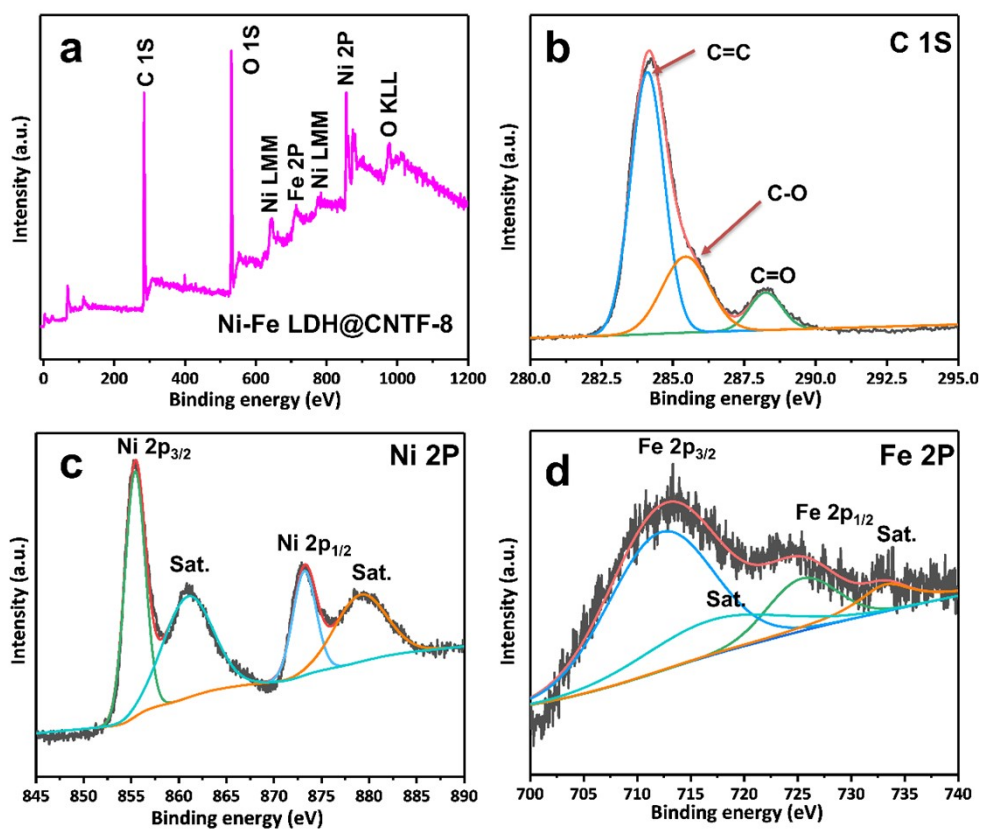


Figure S6. (a) Survey XPS spectrum of Ni-Fe LDH@CNTF-8; (b-d) Corresponding high resolution

XPS spectra of C 1S, Ni 2P and Fe 2P.

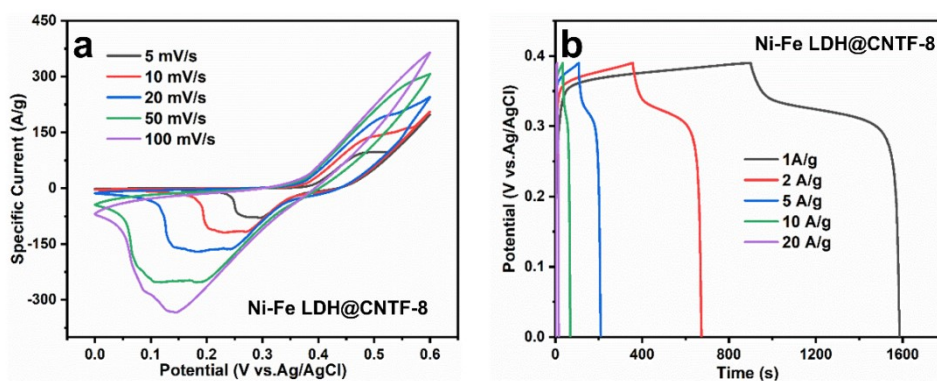


Figure S7. (a) CV and (b) GCD curves of Ni-Fe LDH@CNTF-8 electrode measured at different scan rate and current densities.

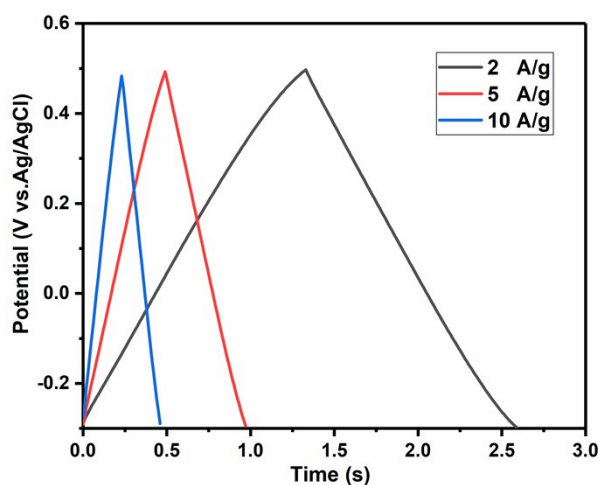


Figure S8. GCD curves of original CNTF at different current densities.

The comparatively rapid change (resulting larger linear slope, Figure S9c) of  $\Delta J$  of Ni-Fe LDH@CNTF-24 sample calculated from the Figure S9a and S9b indicates its higher electrochemical double layer capacitance [10,11]. Based on this, it can be inferred that the hierarchical structure of Ni-Fe LDH@CNTF-24 sample provide more electrochemical active area (ECSA) than that of Ni-Fe LDH@CNTF-8 sample.

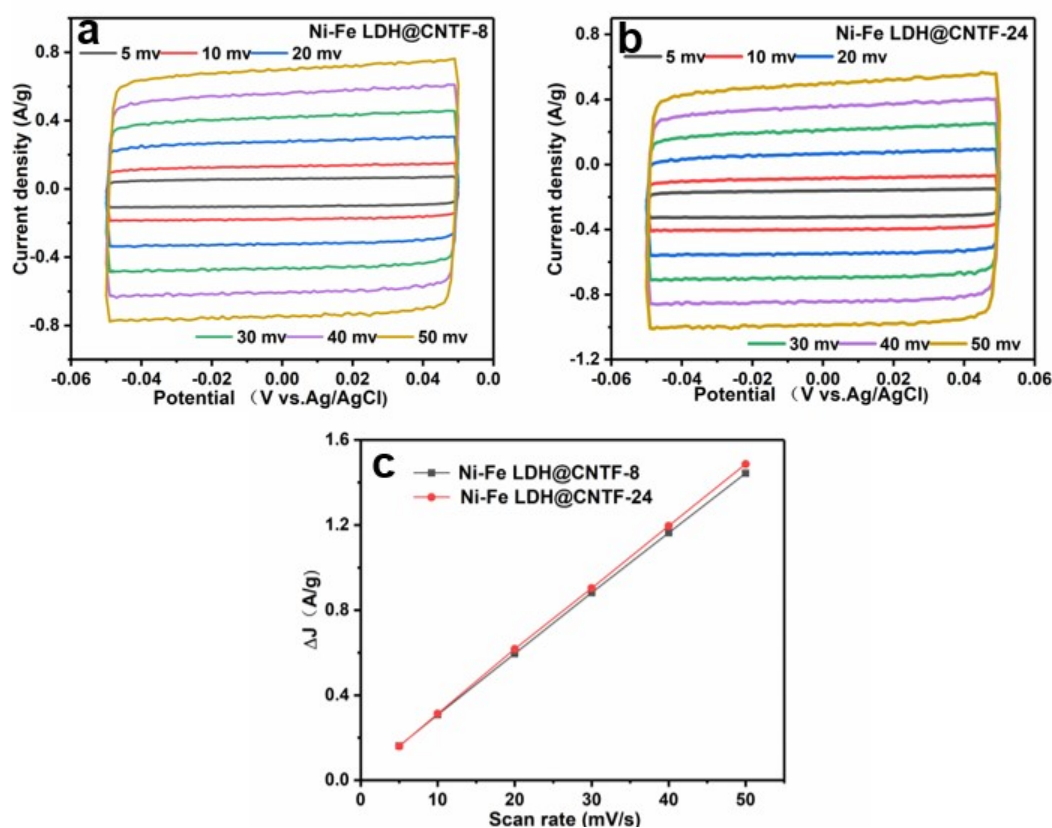


Figure S9. CV curves of (a) Ni-Fe LDH@CNTF-8 and (b) Ni-Fe LDH@CNTF-24 in the potential window of -0.05-0.05 V (vs. Ag/AgCl) at different scanning rates of 5, 10, 20, 30, 40 and 50 mV/s, (c)  $\Delta j$  (=  $j_a$ -  $j_c$ ) plotted against scan rate of Ni-Fe LDH@CNTF-8 and Ni-Fe LDH@CNTF-24.

**Table S1 The resistivity of fiber electrodes**

Name	Original CNTF	Acid treated CNTF	Ni-Fe LDH@CNTF-8	Ni-Fe LDH@CNTF-24
Specific Resistance ( $\Omega/\text{cm}$ )	433.5	154.6	241.4	305.7

### Fabrication of $\text{RuO}_2@\text{CNTF}$

The  $\text{RuO}_2@\text{CNTF}$  were prepared refer to the reported method[12]. Briefly, 60 mg ruthenium chloride hydrate ( $\text{RuCl}_3 \cdot x\text{H}_2\text{O}$ ) was dissolved in 50 ml deionized water with continuous stirring for 0.5 h. Then, the acid treated CNTF were immersed into the solution and transferred to teflon lined stainless steel hydrothermal reactor for 20 h at 180 °C. Subsequently, the as-synthesized fiber sample was washed with DI water and then annealed at 150 °C in air for another 1 h.

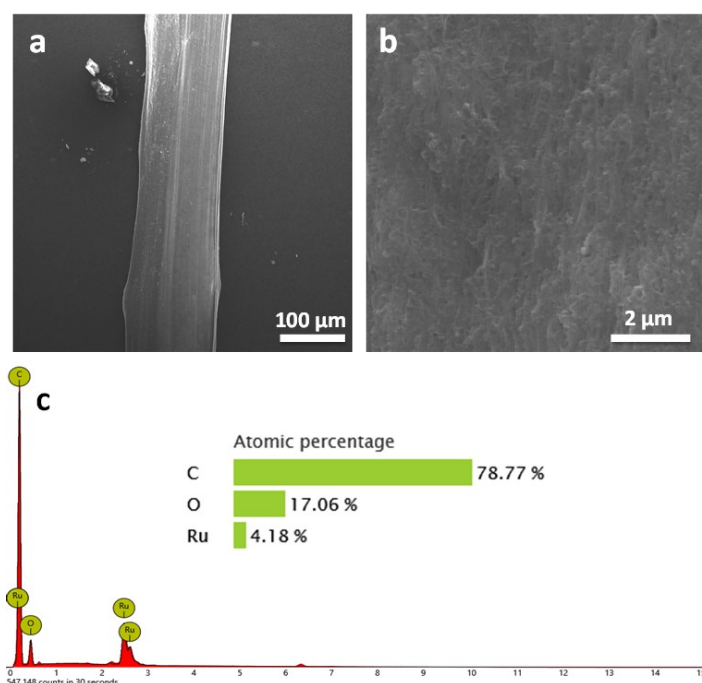


Figure S10. SEM images of  $\text{RuO}_2@\text{CNTF}$  observed at low magnification (a) and high magnification

(b); (c) Corresponding EDX of  $\text{RuO}_2@\text{CNTF}$ .

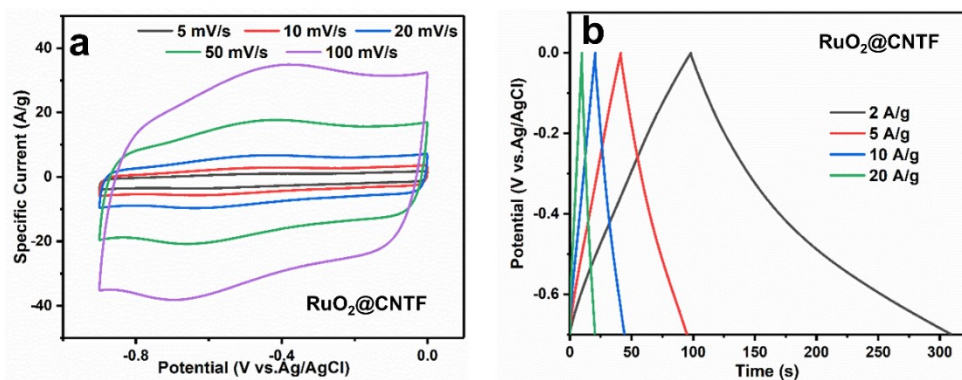


Figure S11. (a) CV and (b) GCD curves of RuO<sub>2</sub>@CNTF at different scan rates and current densities.

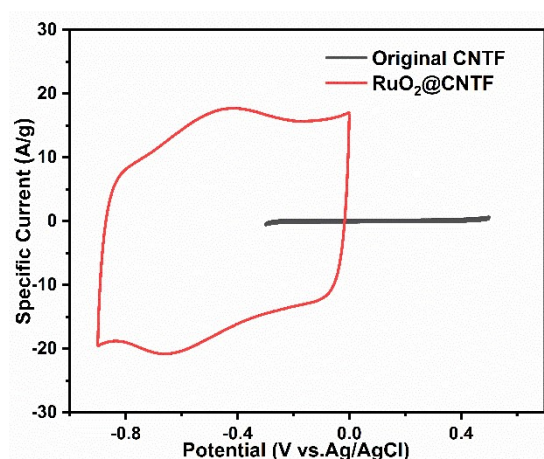


Figure S12. CV curves of original CNTF and RuO<sub>2</sub>@CNTF electrodes measured at scan rate of 50 mV/s.

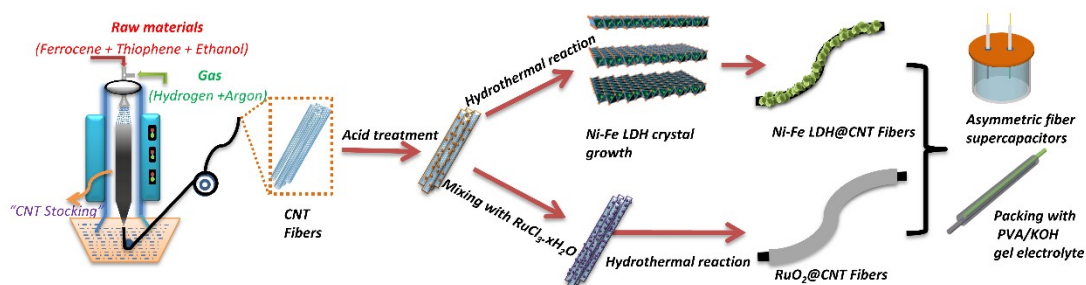


Figure S13. Schematic illustration of the overall fabrication process of ASC (AFSC) based on Ni-Fe LDH@CNTF cathode and RuO<sub>2</sub>@CNTF anode.

## Reference

- [1] T. Brousse, D. Bélanger, J.W. Long, To Be or Not To Be Pseudocapacitive?, *Journal of The Electrochemical Society*. 162 (2015) A5185–A5189.
- [2] T. Brousse, M. Toupin, R. Dugas, L. Athouël, O. Crosnier, D. Bélanger, Crystalline MnO<sub>2</sub> as Possible Alternatives to Amorphous Compounds in Electrochemical Supercapacitors, *Journal of The Electrochemical Society*. 153 (2006) A2171.
- [3] X. Xia, C. Zhu, J. Luo, Z. Zeng, C. Guan, C.F. Ng, H. Zhang, H.J. Fan, Synthesis of free-standing metal sulfide nanoarrays via anion exchange reaction and their electrochemical energy storage application, *Small*. 10 (2014) 766–773.
- [4] Z. Weng, F. Li, D.W. Wang, L. Wen, H.M. Cheng, Controlled electrochemical charge injection to maximize the energy density of supercapacitors, *Angewandte Chemie - International Edition*. 52 (2013) 3722–3725.
- [5] Y. Zhou, Z. Jia, S. Zhao, P. Chen, Y. Wang, T. Guo, L. Wei, X. Cui, X. Ouyang, X. Wang, J. Zhu, J. Sun, S. Pan, Y. Fu, Construction of triple-shelled hollow nanostructure by confining amorphous Ni-Co-S/crystalline MnS on/in hollow carbon nanospheres for all-solid-state hybrid supercapacitors, *Chemical Engineering Journal*. 416 (2021) 129500.
- [6] V. Augustyn, J. Come, M.A. Lowe, J.W. Kim, P.L. Taberna, S.H. Tolbert, H.D. Abruña, P. Simon, B. Dunn, High-rate electrochemical energy storage through Li<sup>+</sup> intercalation pseudocapacitance, *Nature Materials*. 12 (2013) 518–522.
- [7] H.S. Kim, J.B. Cook, H. Lin, J.S. Ko, S.H. Tolbert, V. Ozolins, B. Dunn, Oxygen vacancies enhance pseudocapacitive charge storage properties of MoO<sub>3-x</sub>, *Nature Materials*. 16 (2017)

454–460.

- [8] B. Yao, S. Chandrasekaran, H. Zhang, A. Ma, J. Kang, L. Zhang, X. Lu, F. Qian, C. Zhu, E.B. Duoss, C.M. Spadaccini, M.A. Worsley, Y. Li, 3D-Printed Structure Boosts the Kinetics and Intrinsic Capacitance of Pseudocapacitive Graphene Aerogels, *Adm.* 32 (2020) 1906652.
- [9] X. Wang, Z. Zhou, Z. Sun, J. Hah, Y. Yao, K.S. Moon, J. Di, Q. Li, C. ping Wong, Atomic Modulation of 3D Conductive Frameworks Boost Performance of MnO<sub>2</sub> for Coaxial Fiber-Shaped Supercapacitors, *Nano-Micro Letters.* 13 (2021) 1–12.
- [10] X. Gao, X. Liu, D. Wu, B. Qian, Z. Kou, Z. Pan, Y. Pang, L. Miao, J. Wang, Significant Role of Al in Ternary Layered Double Hydroxides for Enhancing Electrochemical Performance of Flexible Asymmetric Supercapacitor, *Advanced Functional Materials.* 29 (2019) 1–12.
- [11] L. Zhuang, Y. Jia, H. Liu, X. Wang, R.K. Hocking, H. Liu, J. Chen, L. Ge, L. Zhang, M. Li, C.L. Dong, Y.C. Huang, S. Shen, D. Yang, Z. Zhu, X. Yao, Defect-Induced Pt–Co–Se Coordinated Sites with Highly Asymmetrical Electronic Distribution for Boosting Oxygen-Involving Electrocatalysis, *Adm.* 31 (2019) 1–10.
- [12] Q. Jiang, N. Kurra, M. Alhabeab, Y. Gogotsi, H.N. Alshareef, All Pseudocapacitive MXene-RuO<sub>2</sub> Asymmetric Supercapacitors, *Advanced Energy Materials.* 8 (2018) 1703043.